The Photogrammetric Record 25(131): 299–318 (September 2010)

ASSESSMENT OF EROSION, DEPOSITION AND RILL DEVELOPMENT ON IRREGULAR SOIL SURFACES USING CLOSE RANGE DIGITAL PHOTOGRAMMETRY

GIZAW D. GESSESSE* (desta.gizaw@yahoo.com)
HELMUT FUCHS (helmut.fuchs@boku.ac.at)
REINFRIED MANSBERGER (reinfried.mansberger@boku.ac.at)
ANDREAS KLIK (andreas.klik@boku.ac.at)
University of Natural Resources and Applied Life Sciences, Vienna, Austria

DIRK H. RIEKE-ZAPP (zapp@geo.unibe.ch)
University of Bern, Switzerland

*Now at Amhara Region Agricultural Research Institute, Bahir Dar, Ethiopia

Abstract

Understanding the spatial pattern of erosion in inter-rill and rill areas can be useful in locating sources of sediment and in determining down-slope sediment delivery. However, spatial information about erosion processes in the inter-rill and rill areas under field conditions is often limited owing to the non-availability of a detailed microtopography. This paper aims to present a method for the survey of microtopographic soil surface changes caused by erosion and to investigate the development of sediment transport and rill erosion in the inter-rill and rill areas for a given rainfall event. The approach is based on the application of close range digital photogrammetry to produce differences of digital elevation models (DEMs), automatically measured and generated but with manual 3D point editing. Quality analysis of the DEM measurements has shown that erosion and deposition can be detected with a relative error of ±2·8 to ±5·3 mm. The minimum average sediment yield from plots with an area of 53 m^2 after the occurrence of 46 to 70 mm of erosive rainfall was estimated to be 1·24 to 3·5 kg m^{-2}. The spatial pattern of erosion and deposition on inter-rill and rill areas has proved the relative efficiency of rills to transport sediments from inter-rill areas with a sediment delivery ratio greater than one. Thus at erosive rainfall events, the transport capacity of the rill flow was not a limiting condition. The rill network was controlled by abrupt change in surface microtopography where rough surfaces produced many smaller rills but fewer contributing rills than relatively smooth surfaces. Tillage-induced surface roughness, the presence of stones and sparse vegetation, and the borders of individual plots were found to present challenges to the photogrammetric techniques, and to introduce errors which inhibit fully automatic DEM generation. The precision of the DEMs was constrained by the precision of ground control points (GCPs), camera lens distortion towards format edges

and DEM extraction parameters. Despite this limitation, however, the application of digital photogrammetry enabled the measurement of high-frequency microtopographic surfaces and characterisation of the spatial distribution of erosion and deposition and of rill erosion development during highly erosive rainfall events.

KEYWORDS: close range photogrammetry, DEM quality, microtopography, rill density, rill sediment transport

INTRODUCTION

IN ETHIOPIA, SOIL LOSS is mainly associated with extreme rainfall events. Soil surfaces are exposed to extreme erosion because they experience frequent tillage before and during the start of the annual rainy season, at a time when the land has no vegetation cover. On such agricultural lands rill erosion constitutes one of the dominant forms of erosion by water. Estimates from cross-sectional rill surveys have shown that seasonal average soil loss by rills was about 13 to 60 t ha^{-1} from agricultural fields with a range of rill density from 328 to 864 m ha^{-1} (Bewket and Sterk, 2003). Based on the data collected in one of the former Soil Conservation Research Project (SCRP) sites, the mean rill volume and mean rill density were estimated at 60 to 170 m^3 ha^{-1} and 600 to 940 m ha^{-1}, respectively (*source*: SCRP Andit Tid database). Soil erosion rates and sediment yield—specifically at the Angereb subwatersheds—show high variability. Annual erosion rates and sediment yields were in the range of 45 to 200 t ha^{-1} and of 6 to 26 t ha^{-1}, respectively, that resulted in the sediment delivery ratio of 6 to 27% (Admasu, 2005). The estimated mean annual sediment yield at the outlet of the watershed (at the dam site) was 10 to 13·7 t ha^{-1} (Admasu, 2005; Siyam et al., 2005).

Surface sediment transport from hill slopes to river channels is carried out by upstream rill networks. Rill networks are geomorphologically and hydrologically important as sediment transport rates increase rapidly once rill incision occurs (Brunton and Bryan, 2000). Because of the importance of the inter-rill–rill transition, several studies have examined threshold conditions for rill initiation. The transition from inter-rill to rill processes is critical both for erosion rates and the geomorphic evolution of hill slopes (Bryan, 2000). Sediment transport by rill erosion is an integral effect of erosion and deposition on the inter-rill and rill areas. Inter-rill erosion is conceptualised as a process of sediment delivery to concentrated flow or rills, whereby inter-rill sediment is then either carried off by the flow in the rill or deposited on the rill channel. Rill erosion involves flow concentration, often caused on natural hill slopes by microtopography and on agricultural soils by tillage (Bryan, 2000). On freshly cultivated fields, Kirkby (2002) has indicated the effects of rain splash and sediment transport on the reduction of microtopography, which tend to fill depressions at the expense of the higher surfaces, and are more effective in higher frequency microtopography. According to Kirkby, this process is very important in cultivated areas, where plough ridges tend to be poorly consolidated and therefore highly vulnerable. This implies the resulting rills may be randomly or systematically distributed. On such complex topographic surfaces with a micro-rill drainage system not only the transport capacity of the flow but also the microtopography of the areas had an impact on the rill erosion development down slope (Favis-Mortlock, 1998). Govers and Poesen (1988) have shown the change in the relative erosion contributions of inter-rill and rill areas during the development of the drainage network through evolving microtopography. Sediment balance is directly related to erosion if the transport capacity of the rill flow is not exceeded, but it is limited by the transport capacity if erosion exceeds the capacity of the flow (Kinnell, 2004). Understanding the spatial and temporal development of erosion in the inter-rill and rill areas can be useful to locate sources of sediment, the spatial erosion pattern and to

determine the sediment delivery down slope. Studies have been made to consider the spatial and temporal dynamics of sediment delivery within the rill network (Brunton and Bryan, 2000) under different conditions. Brasington and Smart (2003) have also investigated the sediment budget through evolving microtopographic surfaces on experimental basins. Several experiments have been conducted related to inter-rill and rill erosion processes and rill development under laboratory conditions (Loch, 1996; Bryan, 2000; Favis-Mortlock et al., 2000; Rieke-Zapp and Nearing, 2005a, b). However, there is a lack of quantitative information describing the spatial and temporal dynamics of erosion patterns and of sediment transport rates between inter-rill and rill network areas under real field conditions.

Considerable interest exists in the accurate measurement of net loss or gain of soil materials to determine the sediment transport by overland and concentrated linear flow from hill slopes. The measurement of soil loss under field conditions was traditionally based on test plot studies and empirical erosion models. The runoff plot method however is labour-intensive and usually time-consuming. Only large experimental plots conducted over a long period of time can really meet the challenge of obtaining data with proper accuracy and sufficient reliability. Moreover, empirical erosion models are often not suited to complex topography and do not account for deposition. Thus erosion predicted by these models may not be representative of actual conditions and will generally overestimate actual erosion (Mitasova et al., 1998; Jetten et al., 1999; Warren et al., 2000; 2005; Kinnell, 2004).

With an increasing need for spatial and temporal representation of erosion processes, detailed knowledge of microtopographic surface changes in response to rainfall events in order to determine the spatial erosion pattern and associated sediment transport is important. Digital photogrammetry has achieved distinct advantages over conventional field surveying methods for the acquisition of this information, mainly in terms of spatial coverage, accuracy and speed of application. Photogrammetry has been applied for landform representation and for detecting morphological change in the micro-, meso- and macro-scales (Chandler, 1999). Digital photogrammetry integrated with geographical information system (GIS) techniques has contributed to the use of multi-date digital elevation models (DEMs) to estimate spatial erosion patterns and sediment production. The application of stereoscopic photography ranges from the measurement of soil surface roughness characteristics (Rieke-Zapp et al., 2001; Kirkby, 2002; Jester and Klik, 2005; Taconet and Ciarletti, 2007), erosion processes in the rills and gullies (DeRose et al., 1998; Favis-Mortlock et al., 2000; Lascelles et al., 2002; Martinez-Casasnovas et al., 2002; Daba et al., 2003; Rieke-Zapp and Nearing, 2005a, b; Moritani et al., 2006), and river channel morphology and sediment transport rates (Chandler et al., 2001; Brasington and Smart, 2003; Lane et al., 2003). Because of the limitation of photogrammetric accuracy, it was considered that estimation of sediment rates from small-scale morphological change over time was difficult (Chandler et al., 2002). However, Lane et al. (2003) applied a method of DEM difference with estimates of point precision on low-relief gravel-bed rivers and justified reliable levels of detection for erosion and deposition measurements. Brasington and Smart (2003) discussed the use of inverse estimation of sediment transport patterns and rates from analysis of morphological dynamics, which involves inter-comparison of DEMs of surfaces over time. Moritani et al. (2006) have used changes of multi-temporal DEMs to find sheet erosion patterns due to overland flow. However, existing methods of digital photogrammetry that are said to be sufficient to represent detailed microtopographic surfaces have not been commonly applied to tillage-induced microtopography under field conditions.

This paper presents the application of close range photogrammetry to monitor and quantify the change in tillage-induced microtopography by inter-rill and rill erosion using time series of DEM. The objectives of the methodology outlined in this paper are:

(1) to monitor erosion and deposition patterns over time on two different soil textures;
(2) to investigate sediment transport rate and rill erosion development in the inter-rill and rill areas.

MATERIALS AND METHODS

Study Sites

The study site was in the Angereb watershed north of the Lake Tana Basin, Ethiopia. The experiments were conducted from July to August 2008. The seasonal rainfall from June to mid-September was 860 mm. The experimental plots in general represent farmers' tillage practices where tillage-oriented roughness or irregular surface conditions prevail. The photogrammetry experiment was carried out on clay and sandy clay loam textures with an organic carbon content of 2·81 and 2·12%, and bulk density of 1·22 and 1·31 g cm^{-3}, respectively. The slope gradient of the plots was 19 to 21%.

Experimental Set-up and Experimental Conditions

The experiment was conducted on a freshly tilled bare soil surface with plot size of 3·7 m width and 14·4 m length (Figs. 1 and 2). The plots were bounded with corrugated iron sheets inserted 15 cm into the ground and 20 cm above the surface in order to limit the inflow of runoff from outside the plot (Fig. 1). The soil surface of the plots was prepared according to the local tillage practices. Immediately after seedbed preparation and experimental setting, prior to the start of photography, the plots were left for 5 to 7 days in order to allow settling of the loose soil surface. During this period, the plots were pre-wetted with a total natural rainfall of up to 20 mm (individual events of 1·5 to 4·5 mm with an average intensity of 1·5 mm h^{-1}). The acquisition of photographs always started immediately after the occurrence of any high-intensity rainfall event.

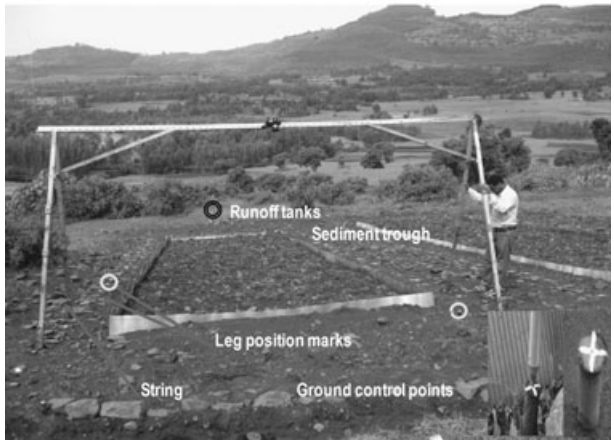

FIG. 1. Field set-up for the photography. Inset shows the detail of a ground control point.

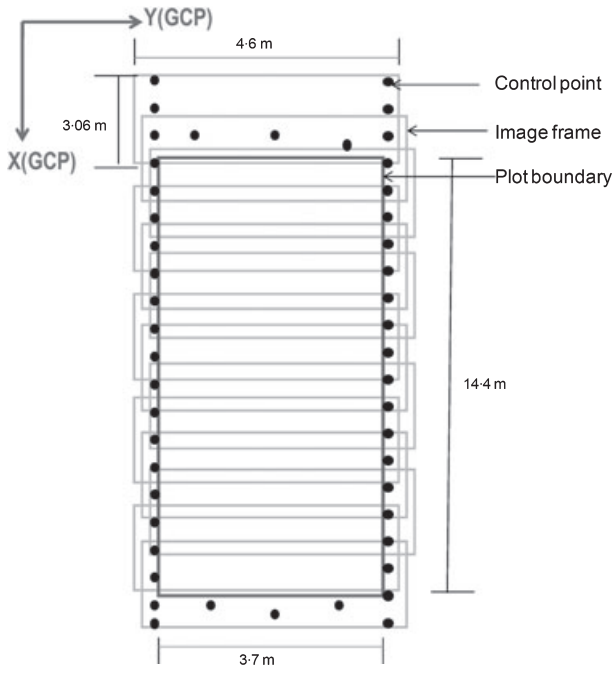

FIG. 2. Diagram showing the photography plan.

Photogrammetric Data Acquisition

The first task was to construct a flexible camera platform system to enable similar photo scales for the whole test site. It was constructed of an aluminium beam and adjustable wooden legs. The camera was firmly mounted to the beam by bolts. Based on the planned photogrammetric set-up the construction was mounted on the predefined frame-stand position marks on the ground (to enable 60% overlap) (Fig. 1). The marked string was used in combination with a plumb bob as an indicator to guarantee the uniformity of the inclination of the camera with respect to the vertical for each camera position.

A calibrated non-metric Canon EOS 1Ds digital camera, with Leica Elmarit 2·8/19 mm ROM lens, was used to acquire overlapping photographs of the whole plot in a time sequence corresponding to extreme rainfall events. The sensor was CMOS with a sensor size of 35·8 mm × 23·8 mm, a pixel size of 8·8 μm and an effective resolution of 4064 × 2704 pixels. The camera was pre-calibrated at a testfield at the University of Bern, Switzerland, using AICON 3D Studio software to assess parameters of interior camera geometry such as focal length, principal point offset and radial symmetric lens distortion (Table I). Post-calibration was made at the same testfield using Photometrix CameraCalibrator. At least 30 images of a three-dimensional testfield with similar dimensions to those of the field soil surface plots were taken for each calibration. There was no possibility for camera calibration during field image acquisition.

The photographs in the field were taken vertically from a height of approximately 2·4 m at an image scale of 1:130. With a focal length of 19 mm a pixel represents 1·13 mm in object space. The whole experimental plot including borders on all sides was covered by a block of

TABLE I. Photographic planning and calibration parameters using Canon EOS 1Ds camera.

Camera parameters	*Values*
Effective pixels	4064 × 2704
Image size, mm	35·8 × 23·8
Pixel size, μm	8·8
Nominal focal length, mm	19
Camera height (*H*), m	2·40
Image scale	1:130
Pixel resolution in object space, mm	1·13
Area per image, m^2	4·60 × 3·06
60% forward overlap, m	1·84
Base distance (*B*), m	1·22

Calibration parameters	*Pre-calibration*	*Rmse*	*Post-calibration*	*SE*
Focal length, mm	18·84113	±0·0775	19·3384	±0·001
X_p, mm	−0·03676	±0·0437	−0·0217	±0·001
Y_p, mm	0·25402	±0·0471	0·2761	±0·001
σ_0, mm		±0·00244		

16 overlapping (60% forward) photographs in one strip (Fig. 2). In order to ensure proper exterior orientation and for the purpose of DEM quality assessment, wooden pegs (8 cm diameter) with white painted crosses with 5 to 8 mm line width, further marked by 4 mm nail heads within the centres of the crosses, were used to target 52 ground control points (GCPs) spaced at approximately 1 m intervals along the boundary of the plot (Fig. 1 inset). The three-dimensional coordinates (*X*, *Y* and *Z*) of the GCPs were collected by conventional terrestrial surveying from two local stations using a SOKKIA Series 30R total station with a point accuracy of 4 mm. In order to optimise the results of DEM generation the photographs were taken under cloud cover to reduce shadows and extreme contrasts in the photographs.

Photogrammetric Orientation and DEM Extraction

Photogrammetric orientation and DEM extraction were performed using the Leica Photogrammetry Suite (LPS, Version 9·3) integrated into ERDAS IMAGINE software (Leica Geosystems, 2005). The photogrammetric orientation was performed by the conventional bundle adjustment procedure with the input of a priori estimated camera positions, automatically generated tie points and manually measured photo coordinates of the GCPs. DEMs were extracted using the LPS automatic tool. The results of this procedure are single mass points in an irregularly spaced network (TIN model) describing the surface. This file format also enables the editing of individual positions and altitudes of mass points and allows the measurement of additional breaklines of the rill network.

To exclude large relief displacements caused by plot border effects during pixel matching (Lane et al., 2003), the area for DEM generation was reduced by 25 cm in advance along the sides and by 50 cm along the top and bottom edges. After undertaking several tests for the two test sites (with two different soil types), to find the optimal strategy (higher search size and increased correlation window size) for automatic DEM measurements, 12 individual TIN surfaces were generated for each of the test sites from overlapping images and merged to form a single block. This procedure was repeated 5 times to access the DEMs of the whole time series.

As the DEM generation tool only measures surface points and the presence of vegetation would falsify the actual soil surface and with it the volume of DEM differences (DeRose et al., 1998), the LPS Terrain Editor was used for manual correction of points generated automatically by the system on vegetated surfaces. To enable the analysis of the DEMs and differences between DEMs in a geographical information system (GIS) the corrected TIN surface models (285 000 to 315 000 point density) were interpolated to a 2 cm grid DEM. Microtopographic soil surface change (or spatial erosion and deposition pattern), rill network and sediment loss information were derived from the grid DEM by means of natural neighbour interpolation in ArcGIS 9·2 (ESRI, 2006).

Assessment of DEM Quality

The accuracy and quality of DEMs collected by photogrammetric techniques is related to the average image scale, the quality of photographs, the accuracy of the interior orientation and of measured GCPs, and the quality of photogrammetric measurements and of the method of aerial triangulation. Additionally the accuracy of the DEMs depends on the quality of the image matching process and the DEM extraction strategy parameters and filter methods (Butler et al., 1998; Walstra, 2006; Wackrow and Chandler, 2008).

Within this project the precision of individual DEMs was evaluated by the residuals of the GCPs, and by the standard deviations of elevation differences between manually measured surface points and automatically derived DEM surfaces. A total of between 1750 and 3075 elevation points from different sampling areas inside the test site were used for quality assessment. The internal DEM errors were checked for normal distribution at 95% confidence interval and independently defined by their means and standard deviations. Systematic errors are caused by errors in the interior and/or exterior orientation and by off-terrain measurements due to vegetation. Because of the difficulty of surveying independent check points inside the plot areas during the experiment, methods similar to those described by DeRose et al. (1998) and Martinez-Casasnovas et al. (2002) were used to identify systematic errors. Sixty to 100 so-called control stones (CSs) per DEM scattered over the whole plot were used to identify systematic errors and relative errors of DEM differences. CSs are stones within the test area which were unaffected by erosion and therefore stable over the complete study period. In order to avoid digitising errors and blunders of the whole CS surfaces, only the top areas of CSs equivalent to one to two grid cells were taken. The evaluation of systematic errors was made by comparing the elevation differences of the CSs. The mean of the elevation differences of the CSs was calculated over multi-date DEMs with reference to the initial (first accessed) DEM and can be seen as an indicator for a systematic error. This value can be used to correct the individual DEMs. Relative errors were identified from the standard deviation of DEM difference of the CSs. Lane et al. (2003) have demonstrated the need to assess the DEM quality in terms of the derived parameters rather than elevation itself, in order to identify a minimum level of detection in the estimation of the parameters. Uncertainty of the erosion and deposition measurements from DEM differences was evaluated using the error propagation method applied by Lane et al. (2003). It involves the pooled variance of individual DEM point precision estimates to detect the minimum level of surface change.

Computation of Erosion, Deposition and Sediment Transport

In a situation where an adequate measurement of hydraulic-process-related parameters (shear stress, sediment load, discharge, velocity) was not possible, an alternative way of erosion

measurement is to estimate the surface change from time series DEMs. The change in the soil surface was measured from differences in the sequential DEMs. In this study the soil loss was not quantified in absolute terms as the surface change is attributed from both soil erosion and settlement due to change in the bulk density. Although 1-week-long pre-wetting was done for the purpose of reducing settling rate, it was assumed that there is uniform settlement rate for the whole surface and the specific erosion and sediment rate were estimated in terms of mass per unit area. After correcting the systematic errors, the spatial difference of initial grid DEM to subsequent time series DEMs produced a cumulative elevation difference grid for each cell. If the height differences were greater than the positive uncertainty these areas were defined as surface erosion. If the height differences were less than the negative uncertainty these areas were defined as surface deposition. Those values within plus or minus the minimum level of detection (or uncertainty) were classified as no change. The specific sediment production rate or the rate of soil surface change was calculated according to the following equation adapted from Rieke-Zapp and Nearing (2005a) and Martinez-Casasnovas et al. (2002):

$$SY = c \cdot Ed \cdot Bd \cdot A \tag{1}$$

where SY is sediment yield produced by the rainfall event (kg), Ed is average elevation difference (m), Bd is bulk density ($\mathrm{kg\,m^{-3}}$), A is the rill and inter-rill area ($\mathrm{m^2}$), and c is the proportionality constant relating the area of trimmed DEM to total plot area.

Through the assessment of the net effect of erosion and deposition, sediment yield was estimated at the rill network system. The rate of sediment production determined at the outlets of the digitised rills was taken as sediment yield ($SY_{i\,+\,r}$) from both inter-rill and rill areas, whereas the amount of net erosion estimated at the head of the same rills was assigned as inter-rill sediment yield (SY_i). Spatial sediment balance between inter-rill and rill areas was based on the input–output mass balance principle (equation (2)). The difference in sediment yield describes the efficiency of rill transport capacity which is measured by sediment delivery ratio (SDR). Analogous to large drainage areas, it is expected that transport capacity is a limiting factor and leads to reduction of sediment yield from inter-rill areas to rill outlets. It was assumed that specific sediment yield declines and the transmission loss increases as the drainage area increases and foreseen sediment delivery ratio is less than one.

$$SY_i = SY_{i+r} + \Delta SY \tag{2}$$

where SY is sediment yield per unit area, and (i) and ($i\ +\ r$) represent inter-rill areas and rill outlets, respectively.

Rill Network Development

Rill density has been used to evaluate the efficiency of rills for sediment transport. The rill density was determined to evaluate the spatial rill erosion variation between soil textures and the temporal development of rill erosion due to soil surface modification in response to rainfall. All rills either with depth exceeding 2 cm or width over 5 cm or length greater than 0·50 m were included in the analysis. An investigation of spatial rill erosion and rill network development was assessed by the rill density, R_d, given in the following equation, calculated by dividing the total length of rill segments (L_r) by the corresponding drainage area (A_r):

$$R_d = \frac{\sum_{1}^{n} L_r}{A_r}. \tag{3}$$

Results and Discussion

Spatial and Temporal Pattern of Erosion and Deposition

As shown in Figs. 3 and 4, the maximum surface change by erosion and deposition was from 80 to 120 mm and 61 to 70 mm for clay soil; and from 63 to 82 mm and 61 to 72 mm for sandy clay loam soil, respectively. Table II shows cumulative amounts of deposition, erosion and sediment production estimated from DEM differences. The rate of sediment deposition and erosion for individual soil textures were comparable. The sum of these values, however, provided a net surface decrease (positive value) due to higher spatial distribution of erosion than deposition. The amount of net erosion was 42·8, 153·7, 154·2 and 376·6 kg for clay; and 52·3, 55·1, 158·8 and 407·6 kg for sandy clay loam soils after the cumulative rainfall of 46, 116, 174 and 410 mm. The corresponding surface changes were 1·02, 3·65, 3·71 and 8·95 mm m^{-2} for clay; and 1·15, 1·43, 4·13 and 9·07 mm m^{-2} for sandy clay loam test sites. During early events, when the initial microtopographic surfaces had greater areas for sediment deposition, erosion rates were lower than those estimated on later occasions with nearly the same rainfall

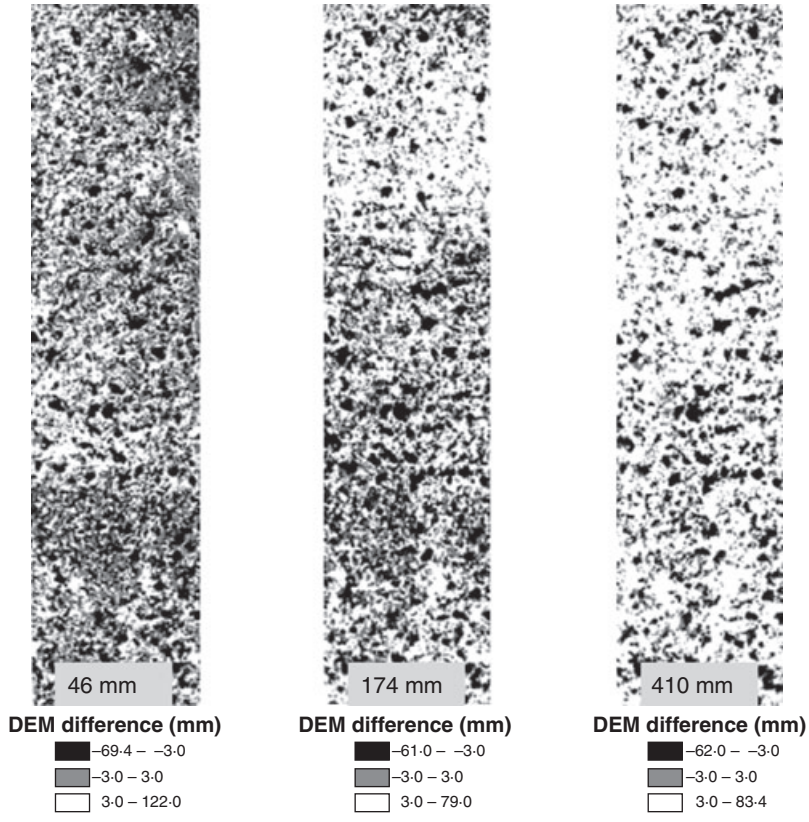

Fig. 3. Soil erosion (white), deposition (black) and no change (grey) pattern for clay soil during cumulative rainfall of 46, 174 and 410 mm.

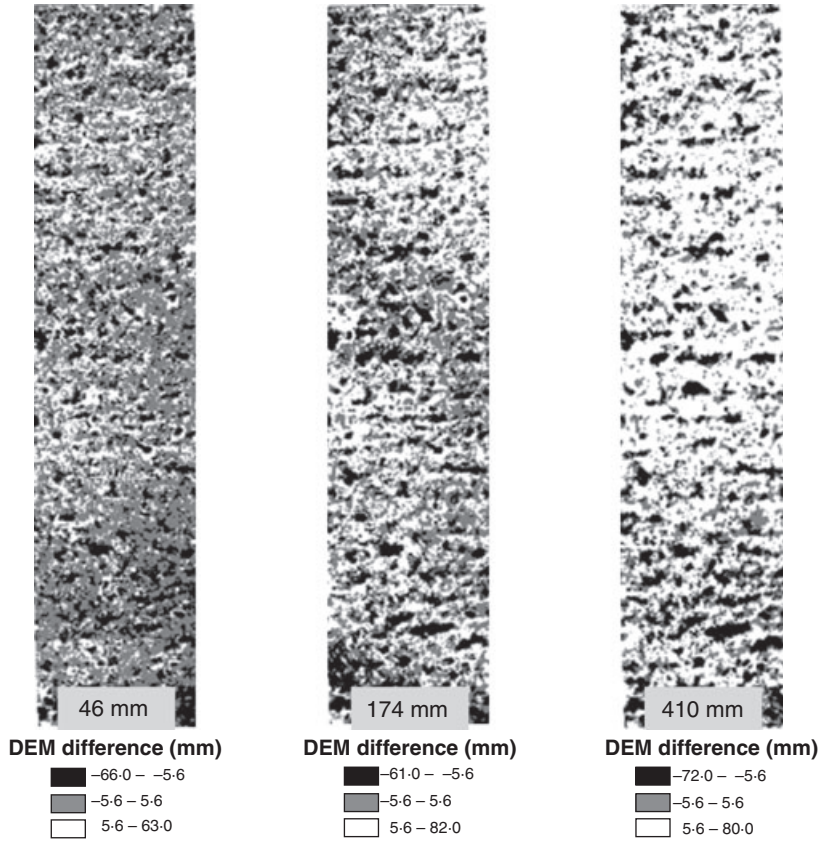

FIG. 4. Soil erosion (white), deposition (black) and no change (grey) pattern for sandy clay loam soil during cumulative rainfall of 46, 174 and 410 mm.

TABLE II. Cumulative deposition, gross erosion and net erosion rates.

DEM difference	*Cumulative rainfall (mm)*	*Relative error (kg)*	*Deposition (kg)*	*Erosion (kg)*	*Net erosion (kg)*
Clay (bulk density Bd = 1·22 g cm^{-3})					
DEM_{16}–DEM_{25}	46	±23·7	113·8	156·6	42·8
DEM_{16}–DEM_{02}	116	±58·3	100·5	254·3	153·7
DEM_{16}–DEM_{06}	174	±159·7	104·3	258·5	154·2
DEM_{16}–DEM_{20}	410	±155·9	71·9	448·5	376·6
Sandy clay loam (bulk density Bd = 1·31 g cm^{-3})					
DEM_{15}–DEM_{25}	46	±60·6	138·9	191·1	52·3
DEM_{15}–DEM_{02}	116	±50·4	163·8	218·9	55·1
DEM_{15}–DEM_{06}	174	±100·6	128·3	287·1	158·8
DEM_{15}–DEM_{20}	410	±167·8	126·9	534·5	407·6

events. The temporal changes in the amount of erosion appeared to be directly related to the proportion of area covered by deposition and erosion. Except in the smallest rainfall event at 46 mm rainfall, the net erosion was higher than the range of relative error.

The minimum average sediment production rate at rainfall events of 46 to 70 mm was estimated to be 1·24 to 3·5 kg m^{-2}. In some cases, because of the temporal surface modification the soil loss rate was as low as 0·40 kg m^{-2}. In the later events with 236 mm total rainfall, the erosion rate was estimated up to 6·5 kg m^{-2}. An immediate increase in sediment yield was observed on clay soils with high initial soil roughness surfaces. This was due to the formation of many smaller rills that contributed to increasing the local sediment transport capacity. Rough soil surfaces were associated with steeper local gradients at which active rill initiation occurred at knick points, where plough ridges tend to be poorly consolidated and therefore highly susceptible (Gómez and Nearing, 2005). Govers et al. (2000) and Kirkby (2002) indicated that rougher surfaces generate greater sediment transport as the roughness elements concentrate the flow and the sediment transport along depressions. This implies that actual erosion can be better estimated if the representation of soil surfaces is more detailed and more accurate. In the Angereb watershed, using the Agricultural Non-Point Source Pollution (AGNPS) model developed by the US Department of Agriculture, with 400 m by 400 m grid cells, Admasu (2005) found average soil loss rates of 0·8 to 1·7 kg m^{-2} from 30 to 50 mm rainfall storms with erosivity of 15 to 30 J m^{-1} h^{-1}. It seems that the actual erosion rates were underestimated at larger grid cell size. This may be because there was no detailed representation of the soil surfaces. Haregeweyn and Yohannes (2003) discuss the improvement of AGNPS model outputs by decreasing grid cell size. Rejman and Brodowski (2005) obtained soil loss rates of 6·69 and 4·95 kg m^{-2} from plots 10 and 20 m long, respectively (which is close to the current research results), after total rainfall of 85 mm with maximum intensity 26 mm h^{-1}. Although further validation with accurate measurement techniques is needed, photogrammetric measurements provided rational soil erosion and deposition estimates for erosive rainfall events studied under agricultural field conditions.

Sediment Transport in the Inter-rill and Rill Areas

As shown in Fig. 5, the sediment yield estimated at rill outlets was higher than the inter-rill area; whereas the sediment deposition rate was higher in the inter-rill area. The rill transport capacity was exceeded during intermediate events and led to sediment deposition for sandy clay loam soil, which might be due to the presence of tillage furrow marks. Increased specific sediment yield at rill outlets showed that there was sediment transport by rill flow and a significant proportion from rill bed erosion too. Sediment transport increased at rill outlets compared to the inter-rill source areas upstream of rills. The sediment delivery ratio at rill outlets was 1 to 1·53 for clay and 0·85 to 1·95 for sandy clay loam. The spatial pattern of erosion and deposition on inter-rill and rill areas has proved the relative efficiency of rills to transport sediments from inter-rill areas with sediment delivery ratio greater than one. Thus the transport capacity of the rill flow was not a limiting condition, and sediment transport losses or sediment deposition occurred largely on inter-rill areas.

Rill Density and Rill Network Development

Rill density has been used as a characteristic indicator of rill erosion and rill network development. Rill network development has been assessed through classifying rills into non-contributing and contributing rills (to the outlet). Rill density was calculated as the ratio of rill length to drainage area, which were acquired automatically using DTMs in the GIS functionality (Table III). The range of rill density for all rills varied from 1·33 to 2·13 m^{-1} (corresponding to 0·75 and 0·45 m rill spacing). However, the average rill density of contributing rills to the outlet was in the range of 0·60 to 0·85 m^{-1} (corresponding to 1·65 to

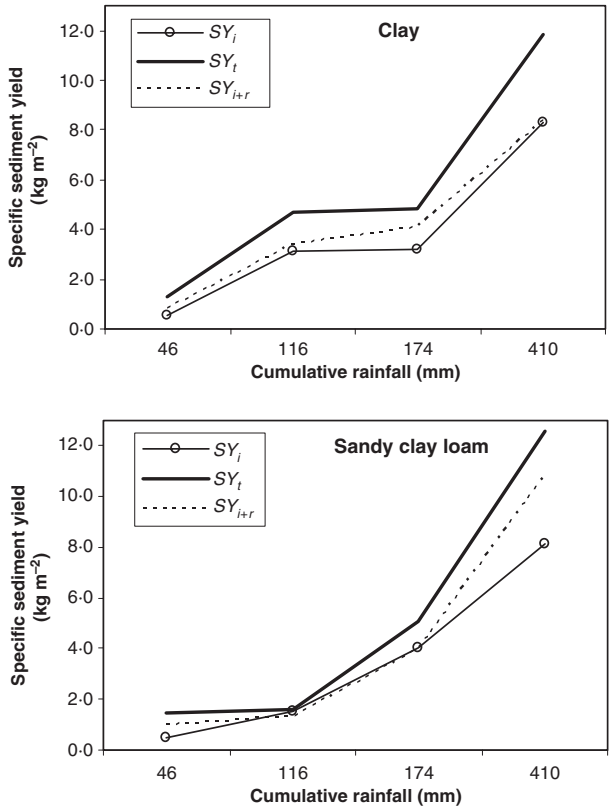

FIG. 5. Specific sediment yield from inter-rill area (SY_i), rill outlet (SY_{i+r}) and whole plot area (SY_t).

TABLE III. Mean rill density (m^{-1}) of all and contributing rills on clay and sandy clay loam soils.

Soil texture	*Cumulative rainfall (mm)*	*Contributing rills*	*All rills*
Clay	46	0·69	2·05
	116	0·75	2·13
	174	0·61	2·03
	410	0·85	2·10
	Mean	0·72	2·08
Sandy clay loam	46	0·69	1·48
	116	0·73	1·33
	174	0·74	1·79
	410	0·75	1·81
	Mean	0·73	1·62

1·20 m rill spacing) and more or less equal on both soil textures. Rejman and Brodowski (2005) have found numbers of rills deeper than 0·50 cm in the range of 2·6 to 3·5 m^{-1} on a high silt content plot of 3 m width. If small rills had been included in the current study, the total numbers of rills would seem likely to have been comparable with the rill numbers found by Rejman and Brodowski (2005).

Discrepancies in rill densities between all rills and contributing rills have indicated the role of microtopography in the formation of rills and the rill network. For example, clay soil with relatively high soil roughness has generated more small rills which merged into a few larger rills draining out of the plot, compared to sandy clay loam soils (Table III). For clay soils, cohesion of freshly wetted surface soil is extremely low, so that the critical shear stress of the soil is close to zero, and rills initiate at extremely low discharges (Loch, 1996). Such soils are characterised by high rilling and a low threshold for rill development.

The higher the soil surface roughness, the larger the density of smaller rills will be and the number of contributing rills to the outlet will be fewer. This implies that rill density and rill network development are controlled by the distribution of the soil surface microtopography and by abrupt changes in it. Rill networks were developed as a result of the interconnection of soil surface depressions when flow concentrates in the channels. The presence and distribution of the depressions led to the confluence of rills and networks of rills. Generally, the assessment and measurement of rill erosion in terms of rill density at both spatial and temporal scales can help to characterise rill erosion and describe spatial distribution of rill erosion semi-quantitatively.

Quality of DEM

The derived DEMs represent microtopographic soil surface or tillage roughness, which is characterised by initial random roughness of 6·4 and 4·6 cm for clay and sandy clay loam soils, respectively. The accuracy of photogrammetric measurements and extracted DEMs is presented in relation to tie point precision, GCPs, photogrammetric bundle block adjustment, automatic DEM generation and independent check points.

Table IV shows the tie point precision in the object space, accuracy of bundle adjustment and GCPs. The root mean square error (rmse) of the photogrammetric solution or the least squares estimation of the bundle adjustment was on average 0·0027 mm, at image scale. An outlined maximum rmse of ±2·6 mm and of ±4·8 mm was estimated for the GCPs from the bundle adjustment on clay and sandy clay loam soil textures. The low precision of the GCPs was possibly attributed to the relative precision of GCP coordinate measurements (±4·0 mm in all dimensions) by the total station and may also be attributed to the geometric stability of the camera which was calibrated once before the experiments. The calibration model of a camera

TABLE IV. Root mean square error of bundle adjustment, tie points and GCPs.

Soil texture	*Multi-date DEM*	*Rmse of bundle adjustment (mm)*	*Rmse of tie points (mm)*		*Rmse of GCPs (mm)*		
			X and Y	*Z*	*X*	*Y*	*Z*
Clay	16 July 2008	0·00264	1·10	1·50	2·50	1·80	2·20
	25 July 2008	0·00277	1·20	1·60	2·50	1·60	2·60
	2 August 2008	0·00273	1·20	1·70	2·10	2·20	1·80
	6 August 2008	0·00281	1·20	1·60	2·10	2·10	2·20
	20 August 2008	0·00250	1·00	1·40	2·70	1·80	1·30
	Average	**0·00269**	**1·14**	**1·56**	**2·38**	**1·90**	**2·02**
Sandy clay loam	15 July 2008	0·00274	1·20	1·60	2·50	3·20	3·40
	25 July 2008	0·00233	1·00	1·40	5·00	3·40	4·30
	2 August 2008	0·00278	1·30	1·70	3·70	3·70	4·40
	6 August 2008	0·00289	1·30	1·70	3·20	4·00	4·50
	20 August 2008	0·00252	1·10	1·50	3·70	4·00	4·80
	Average	**0·00265**	**1·20**	**1·58**	**3·62**	**3·66**	**4·28**

typically deteriorates towards the edges which may also have an effect on accuracy in the image areas where GCPs were measured. The precision of GCPs was up to 3 times worse than the precision of tie points with ±1·60 mm in the object space. The vertical precision expected from the set-up of the Canon EOS 1Ds camera was calculated by multiplying the height-to-base ratio (2·0) with the precision of point measurements in image space (which varies for different DEMs) and the image scale number (130) (Rieke-Zapp and Nearing, 2005b). The resulting values are approximately 3 times better than the precision achieved for tie points (on

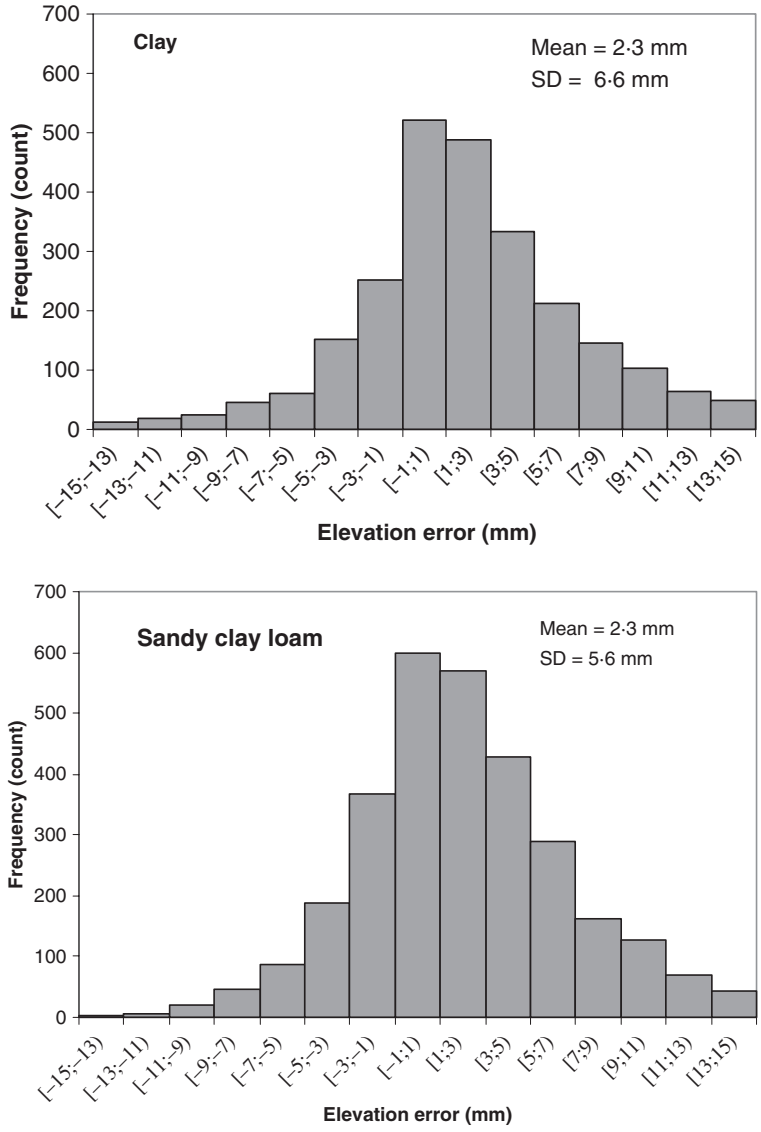

FIG. 6. Histogram of elevation errors between manually digitised points and DEM points for clay and sandy clay loam soils.

average 1·57 mm). The constraint on the accuracy or absolute precision of the extracted DEM was therefore related to the low precision of 3D coordinates of GCPs and to image matching problems in the border areas due to edge effects.

Mass point matching quality is one of the qualitative criteria in assessing automatically extracted DEMs. Before excluding the erroneous points automatically generated on grass surfaces, point matching quality has shown less than 15% unsuccessful matching. The mismatching was mainly observed towards the edges of the plots, on the surfaces of stones forming peaks, and on deep surface depressions where there was low contrast. At this stage the 3D points were subjected to manual editing and subsequent interpolation on the constrained areas.

The mean error of elevation differences between manually measured independent surface points and the DEM surface was +2·3 mm. The corresponding standard deviations of error were ±6·6 and ±5·6 mm for the clay and sandy clay loam test sites, respectively. The histogram of elevation differences approximately fits the normal distribution at 95% significance level (Fig. 6). The mean error of individual DEMs indicates that the derived surface model was systematically lower than the actual surface. The downgraded internal precision of DEMs was partly due to the point mismatching constraints on specific peaks and depressions. Visualisation of the DEM point generation showed that the main contribution for the underestimation emerged from the use of filtering functions and the set of strategies for DEM extraction. High offset mainly occurred on peak surfaces such as stones and soil clods, and in deep sinks. Since the objective was to measure the relative soil surface change and sediment loss from DEM differences, the absolute error cancelled out.

The mean of the systematic error was 3·3 to 5·4 mm for clay and 0·2 to 2·7 mm for sandy clay loam soils as presented in Table V. The respective time series DEMs were corrected by adding the corresponding mean error. The standard deviation of elevation differences of the CSs was, on average, ±2·75 mm for clay and ±5·33 mm (1 σ) for sandy clay loam textures. These point precision values are relative errors to measure erosion and deposition over successive rainfall periods. The greater relative error for sandy clay loam soil was related to the increased residual error of GCPs in Table IV.

Uncertainty of DEM differences was obtained using pooled standard deviations of individual DEM point precision estimates. Accordingly, the average order of magnitude of uncertainties identified to detect minimum level deposition or erosion was estimated at ±2·98 and ±5·64 mm. The minimum level of detection was used to classify deposition, erosion and "no change" amounts. For all of the rainfall events studied, the deposition or erosion rates can be detected significantly. The spatial area coverage of erosion and deposition was different (Figs. 3 and 4). The distribution of the DEM differences in the range of the uncertainty values is skewed to negative values (Fig. 7). Thus, the percentage of deposition areas lost (classified into no change area) was high compared to erosion area; and resulted in slight increase in net

TABLE V. Mean and standard deviation (SD) of error of the control stones (CSs).

Clay			*Sandy clay loam*		
DEM difference	*Mean (mm)*	*SD (mm)*	*DEM difference*	*Mean (mm)*	*SD (mm)*
DEM_{16}–DEM_{25}	3·30	2·50	DEM_{15}–DEM_{25}	0·20	5·10
DEM_{16}–DEM_{02}	4·80	2·80	DEM_{15}–DEM_{02}	1·10	5·00
DEM_{16}–DEM_{06}	4·40	2·90	DEM_{15}–DEM_{06}	0·30	5·40
DEM_{16}–DEM_{20}	5·40	2·80	DEM_{15}–DEM_{20}	2·70	5·80
Average	4·48	2·75	Average	1·08	5·33

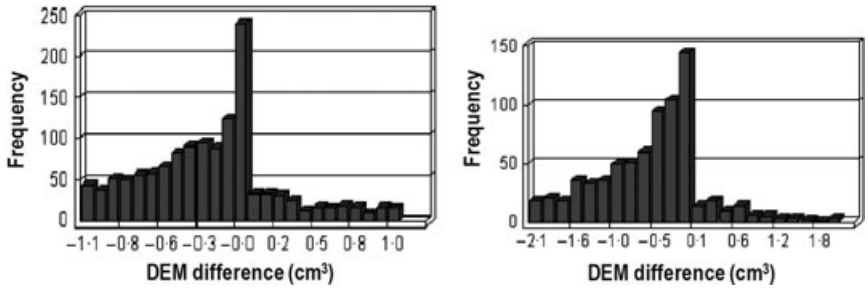

FIG. 7. Distribution of DEM differences within the range of uncertainty values for clay and sandy clay loam soils.

erosion after adjusting to the uncertainty. This implies that deposition areas were less detectable. However, through further improvements in the photogrammetric system and in the precision of three-dimensional GCP coordinates a better level of detection would be achieved.

CONCLUSION

Local microtopography controls the erosion processes and rill network development. High rough surfaces induced by conventional tillage generate, compared to relatively smooth surfaces, greater erosion rates and more small rills. Surfaces with large numbers of small rills produced high sediment yields. Rill sediment transport capacity is not limited and results in a sediment delivery ratio greater than one at rill outlets. Representing detailed soil surface roughness (for example, at cm scale) could improve the estimation of actual erosion and deposition rates.

Analysis of various areas at study sites has shown that high local microtopography due to the presence of tillage roughness, stones and vegetation, low contrast areas such as plot border areas, deep shadows on depression areas and low numbers of points on less decomposed grass clods and flat stone surfaces all produce false peaks and pits and eventually affect the accuracy of photogrammetric measurements of soil erosion in field studies. The measurement precision with the existing photogrammetric scale does not allow monitoring of erosion processes involved for every rainfall event. With highly erosive storms, however, significant erosion and deposition rates can be measured after correction for uncertainty. A better accuracy in the measurements would be achieved through further improving the photogrammetric scale, camera stability and ground control precision. Generally, the proposed method can help to fill the gap in current field methods and characterise statistically significant erosion and deposition rates, inter-rill and rill sediment transport and rill network development at a high level of spatial detail under extreme rainfall events in field conditions with acceptable accuracy. Since runoff plot erosion measurement inevitably includes large potential sources of error, the proposed method could enhance field soil erosion research. Indeed, further research is suggested to validate this application of photogrammetry under field conditions, by improving the accuracy of ground control measurements and camera stability, with the aim of improving the accuracy of field erosion measurement.

ACKNOWLEDGEMENTS

The authors gratefully acknowledge the Austrian Development Cooperation (ADC) within the North-South-Dialogue Scholarship program for the first author's Ph.D. study grant.

REFERENCES

ADMASU, A., 2005. *Study of sediment yield from the watershed of Angereb reservoir*. M.Sc. Thesis, Alemaya University, Ethiopia. 98 pages.

BEWKET, W. and STERK, G., 2003. Assessment of soil erosion in cultivated fields using a survey methodology for rills in the Chemoga watershed, Ethiopia. *Agriculture, Ecosystems & Environment*, 97(1–3): 81–93.

BRASINGTON, J. and SMART, R. M. A., 2003. Close range digital photogrammetric analysis of experimental drainage basin evolution. *Earth Surface Processes and Landforms*, 28(3): 231–247.

BRUNTON, D. A. and BRYAN, R. B., 2000. Rill network development and sediment budgets. *Earth Surface Processes and Landforms*, 25(7): 783–800.

BRYAN, R. B., 2000. Soil erodibility and processes of water erosion on hillslope. *Geomorphology*, 32(3–4): 385–415.

BUTLER, J. B., LANE, S. N. and CHANDLER, J. H., 1998. Assessment of DEM quality for characterizing surface roughness using close range digital photogrammetry. *Photogrammetric Record*, 16(92): 271–291.

CHANDLER, J. H., 1999. Effective application of automated digital photogrammetry for geomorphological research. *Earth Surface Processes and Landforms*, 24(1): 51–63.

CHANDLER, J. H., SHIONO, K., RAMESHWAREN, P. and LANE, S. N., 2001. Measuring flume surfaces for hydraulics research using a Kodak DCS460. *Photogrammetric Record*, 17(97): 39–61.

CHANDLER, J., ASHMORE, P., PAOLA, C., GOOCH, M. and VARKARIS, F., 2002. Monitoring river-channel change using terrestrial oblique digital imagery and automated digital photogrammetry. *Annals of the Association of American Geographers*, 92(4): 631–644.

DABA, S., RIEGER, W. and STRAUSS, P., 2003. Assessment of gully erosion in eastern Ethiopia using photogrammetric techniques. *Catena*, 50(2–4): 273–291.

DEROSE, R. C., GOMEZ, B., MARDEN, M. and TRUSTRUM, N. A., 1998. Gully erosion in Mangatu Forest, New Zealand, estimated from digital elevation models. *Earth Surface Processes and Landforms*, 23(11): 1045–1053.

ESRI, 2006. *ArcGIS 9.2*. Environmental System Research Institute (ESRI), Redlands, California. Pagination unknown.

FAVIS-MORTLOCK, D. T., 1998. A self-organising dynamic systems approach to the simulation of rill initiation and development on hillslopes. *Computers and Geosciences*, 24(4): 353–372.

FAVIS-MORTLOCK, D. T., BOARDMAN, J., PARSONS, A. J. and LASCELLES, B., 2000. Emergence and erosion: a model for rill initiation and development. *Hydrological Processes*, 14(11–12): 2173–2205.

GÓMEZ, J. A. and NEARING, M. A., 2005. Runoff and sediment losses from rough and smooth soil surfaces in a laboratory experiment. *Catena*, 59(3): 253–266.

GOVERS, G. and POESEN, J., 1988. Assessment of the interrill and rill contributions to total soil loss from an upland field plot. *Geomorphology*, 1(4): 343–354.

GOVERS, G., TAKKEN, I. and HELMING, K., 2000. Soil roughness and overland flow. *Agronomie*, 20(2): 131–146.

HAREGEWEYN, N. and YOHANNES, F., 2003. Testing and evaluation of agricultural non-point source pollution model (AGNPS) on Augucho catchment, western Hararghe, Ethiopia. *Agriculture, Ecosystem & Environment*, 99(1–3): 201–212.

JESTER, W. and KLIK, A., 2005. Soil surface roughness measurement—methods, applicability, and surface representation. *Catena*, 64(2–3): 174–192.

JETTEN, V., DE ROO, A. and FAVIS-MORTLOCK, D., 1999. Evaluation of field-scale and catchment-scale soil erosion models. *Catena*, 37(3–4): 521–541.

KINNELL, P. I. A., 2004. Sediment delivery ratios: a misaligned approach to determining sediment delivery from hillslopes. *Hydrological Processes*, 18(16): 3191–3194.

KIRKBY, M., 2002. Modelling the interactions between soil surface properties and water erosion. *Catena*, 46(2–3): 89–102.

LANE, S. N., WESTAWAY, R. M. and HICKS, D. M., 2003. Estimation of erosion and deposition volumes in a large, gravel-bed, braided river using synoptic remote sensing. *Earth Surface Processes and Landforms*, 28(3): 249–271.

LASCELLES, B., FAVIS-MORTLOCK, D. T., PARSONS, A. J. and BOARDMAN, J., 2002. Automated digital photogrammetry: a valuable tool for small-scale geomorphological research for the non-photogrammetrist? *Transactions in GIS*, 6(1): 5–15.

LEICA GEOSYSTEMS., 2005. *Leica Photogrammetry Suite. User's Guide*. Leica Geosystems Geospatial Imaging, Norcross, Georgia. Pagination unknown.

LOCH, R. J., 1996. Using rill/interrill comparisons to infer likely responses of erosion to slope length: implications for land management. *Australian Journal of Soil Research*, 34(4): 489–502.

MARTINEZ-CASASNOVAS, J. A., RAMOS, M. C. and RIBES-DASI, M., 2002. Soil erosion caused by extreme rainfall events: mapping and quantification in agricultural plots from very detailed digital elevation models. *Geoderma*, 105(1–2): 125–140.

MITASOVA, H., MITAS, L., BROWN, W. M. and JOHNSTON, D. M., 1998. *Multidimensional soil erosion/deposition modeling and visualization using GIS*. Final report for USA CERL. University of Illinois, Urbana-Champaign, Illinois. http://skagit.meas.ncsu.edu/~helena/gmslab/reports/cerl98/cerlrep98.html [Accessed: 2nd June 2010].

MORITANI, S., YAMAMOTO, T., HENINTSOA, A. and MURAKI, H., 2006. Monitoring of soil erosion using digital camera under simulated rainfall. *Transactions, Japanese Society of Irrigation, Drainage and Reclamation Engineering*, 74(4): 143–150.

REJMAN, J. and BRODOWSKI, R., 2005. Rill characteristics and sediment transport as a function of slope length during a storm event on loess soil. *Earth Surface Processes and Landforms*, 30(2): 231–239.

RIEKE-ZAPP, D. H., WEGMANN, H., SANTEL, F. and NEARING, M. A., 2001. Digital photogrammetry for measuring soil surface roughness. *Proceedings of the American Society of Photogrammetry & Remote Sensing 2001 Conference: Gateway to the New Millennium*, St Louis, Missouri. 8 pages.

RIEKE-ZAPP, D. H. and NEARING, M. A., 2005a. Slope shape effects on erosion: a laboratory study. *Soil Science Society of America Journal*, 69(5): 1463–1471.

RIEKE-ZAPP, D. H. and NEARING, M. A., 2005b. Digital close range photogrammetry for measurement of soil erosion. *Photogrammetric Record*, 20(109): 69–87.

SIYAM, A. M., EL ZEIN, S., EL SAYED, S. M., MIRGHANI, M. and GOLLA, S., 2005. *Assessment of the current state of Nile Basin reservoir sedimentation problem*. Nile Basin Capacity Building Network (NBCBN), River morphology research cluster (Group 1), Addis Ababa, Ethiopia. 73 pages.

TACONET, O. and CIARLETTI, V., 2007. Estimating soil roughness indices on a ridge-and-furrow surface using stereo photogrammetry. *Soil and Tillage Research*, 93(1): 64–76.

WACKROW, R. and CHANDLER, J. H., 2008. A convergent image configuration for DEM extraction that minimises the systematic effects caused by an inaccurate lens model. *Photogrammetric Record*, 23(121): 6–18.

WALSTRA, J., 2006. *Historical aerial photographs and digital photogrammetry for landslide assessment*. Ph.D. Thesis, Loughborough University. 247 pages.

WARREN, S. D., MITASOVA, H., JOURDAN, M. R., BROWN, W. M. and JOHNSON, B. E., 2000. *Digital terrain modelling and distributed soil erosion simulation/measurement for minimizing environmental impacts of military training*. Center for Ecological Management of Military Lands TPS 00-2. Colorado State University, Fort Collins College of Forestry and Natural Resources. 76 pages.

WARREN, S. D., MITASOVA, H., HOHMANN, M. G., LANDSBERGER, S., ISKANDER, F. Y., RUZYCKI, T. S. and SENSEMAN, G. M., 2005. Validation of a 3-D enhancement of the universal soil loss equation for prediction of soil erosion and sediment deposition. *Catena*, 64(2–3): 281–296.

Résumé

La compréhension de l'organisation spatiale de l'érosion dans et entre les zones de ravinement permet de localiser les sources de sédiments et de déterminer l'apport sédimentaire au pied des versants. Cependant, l'information spatiale sur les processus érosifs est souvent limitée en raison d'une microtopographie mal connue. Cet article présente une méthode de relevé des changements microtopographiques de la surface du sol causés par l'érosion et d'étudier les processus de transport sédimentaire et d'érosion dans et entre les zones de ravinement pour un événement pluvieux donné. L'approche s'appuie sur des différences de modèles numériques de terrain (MNT), déterminés automatiquement par photogrammétrie terrestre, avec édition ultérieure des points 3D par l'opérateur. Le contrôle de qualité des mesures issues du MNT montre que l'érosion et la sédimentation peuvent être détectées avec une erreur relative de ±2,8 à 5,3 mm. L'apport sédimentaire moyen sur des surfaces de 53 m^2 consécutif à des pluies érosives de 46 à 70 mm est estimé à 1,24 à 3,5 kg m^{-2}. L'organisation spatiale de l'érosion et de la sédimentation montre la relative efficacité des ravines pour transporter les sédiments depuis les zones inter-ravines avec un taux d'apport sédimentaire supérieur à 1. Ainsi, en cas d'événement pluvieux érosif, la capacité de transport du flux de ruissellement n'est pas une condition limitante. Le réseau de ravines est contrôlé par des changements brutaux de la microtopographie de surface, les surfaces rugueuses produisant des ravines plus nombreuses, plus petites et ayant une moindre contribution au transport sédimentaire

que les surfaces relativement lisses. La rugosité de surface induite par les labours, la présence de pierres et de végétation clairsemée, et les bordures des parcelles étudiées posent des difficultés pour les techniques photogrammétriques, et entraînent des erreurs qui empêchent la production automatique de MNT. La précision des MNT est limitée par la précision des points d'appui, les distorsions de l'optique en bordure de champ et les paramètres d'extraction du MNT. Cependant, malgré ces limitations, l'utilisation de la photogrammétrie numérique permet de mesurer les hautes fréquences de la microtopographie de surface et de caractériser l'érosion et la sédimentation ainsi que les processus de ravinement pendant des événements pluvieux très érosifs.

Zusammenfassung

Das Verständnis räumlich verteilter Erosionsmuster kann für die Ausweisung von Erosionsflächen und zur Beschreibung des Sedimenttransportes hilfreich sein. Diese räumlichen Informationen über Prozesse in Inter-rill- und Rillenbereichen sind zumeist aber aufgrund fehlender Verfügbarkeit mikrotopografischer Bodenaufnahmen begrenzt. Ziel dieser Studie war es, (1) eine Methode zur Erfassung erosionsbedingter mikrotopografischer Veränderungen der Bodenoberfläche zu erarbeiten und (2) die Entwicklung von Rillenerosion und den Sedimenttransport in Rillen- und Inter-rill-Bereichen zu untersuchen. Der Ansatz basiert auf dem Vergleich unterschiedlicher digitaler Höhenmodelle (DHM), welche von komplexen Bodenoberflächen mit Hilfe der Nahbereichsphotogrammetrie generiert wurden. Qualitätsanalysen der DHM zeigten, dass mikrotopografische Bodenveränderungen infolge erosiver Niederschläge mit einem relativen Fehler von ±2·8 bis ±5·3 mm signifikant erfasst werden können. Der geringste mittlere Sedimentaustrag aus 53 m^2 großen Erosionsplots betrug nach Starkniederschlägen von 46 bis 70 mm 1·24 bis 3·5 kg m^{-2}. Das räumliche Muster von Erosion und Deposition in den Zwischenrillenbereichen bestätigte, dass keine transportlimitierenden Zustände auftraten und das Sediment in den Rillen abtransportiert werden konnte. Die Transportkapazität des Abflusses in den Rillen wurde nie zum limitierenden Faktor. Das Rillennetzwerk wurde wesentlich durch abrupte Änderungen der Oberflächenmikrotopografie beeinflusst, da Oberflächen mit hoher Rauhigkeit eine größere Anzahl von Rillen aber weniger durchgängige Rillen hervorriefen, als solche mit geringer. Die Anwendung digitaler Photogrammetrie ermöglichte die Messung bzw. Erfassung erosionsbedingter mikrotopografischer Veränderungen von Bodenoberflächen und die Charakterisierung von Erosion und Deposition, von Inter-rill- und Rillenerosion sowie das Auftreten und die Entwicklung von Erosionsrillen in einem detaillierten zeitlichen Maßstab während erosiver Regenereignisse.

Resumen

La identificación del patrón espacial de la erosión en áreas de cárcavas y áreas entre cárcavas puede ser útil para localizar el origen del sedimento y determinar la cantidad de sedimento acumulado en la base. Sin embargo la información espacial de los procesos erosivos en áreas de cárcavas y áreas entre cárcavas en condiciones de campo es limitada por la carencia de una microtopografía detallada. Este artículo tiene como objetivo proponer un método para medir los cambios microtopográficos en la superficie del suelo causados por la erosión e investigar la evolución del

transporte de sedimento y la erosión en cárcavas en áreas de cárcavas y entre cárcavas para un determinado episodio de precipitación. Este enfoque se apoya en las diferencias existentes entre modelos digitales de elevación (MDE) calculados y obtenidos automáticamente mediante la edición manual de los puntos tridimensionales aplicando los métodos de la fotogrametría digital de objeto cercano. El análisis de calidad de los MDE señala que tanto la erosión como la sedimentación se pueden detectar de forma reveladora con un error relativo comprendido entre ±2,8 y ± 5,3 mm. Se estima que la generación mínima media de sedimento en parcelas con un área de 53 m^2 tras una precipitación erosiva de 70 mm está entre 1,24 y 3,5 kg m^{-2}. El patrón espacial de erosión y deposición en áreas de cárcavas y áreas entre cárcavas ha demostrado la eficiencia relativa de las cárcavas en el proceso de transporte de sedimentos desde las áreas entre cárcavas con una ratio de producción de sedimento mayor de uno. Así, en episodios de precipitación erosiva la capacidad de transporte de la cárcava no es una condición limitante. La red de cárcavas se controló midiendo los cambios bruscos en la microtopografía superficial, de modo que las superficies rugosas produjeron más cárcavas menores pero menos cárcavas contribuyentes que en las superficies relativamente más suaves. El cultivo favorece la rugosidad de la superficie, la presencia de piedras y la cubierta con vegetación dispersa, y los bordes de las parcelas individuales supusieron un desafío para las técnicas fotogramétricas induciendo errores que frenaron el cálculo completamente automático de un MDE. La precisión de los MDE se vio limitada por la precisión de los puntos de apoyo terrestre, la distorsión de la lente de la cámara hacia los bordes y los parámetros de extracción de los MDE. Sin embargo, pese a esta limitación, la aplicación de la fotogrametría digital permitió la medida de superficies microfotográficas de alta frecuencia y la caracterización de la distribución espacial de la erosión y la deposición, y la medida de la evolución de la erosión en las cárcavas durante episodios de precipitación fuertemente erosivos.